PLOS ONE

RESEARCH ARTICLE

Reproducibility of magnetic resonance fingerprinting-based T_1 mapping of the healthy prostate at 1.5 and 3.0 T: A proof-of-concept study

Nikita Sushentsev[1☯]*, Joshua D. Kaggie[1☯], Rhys A. Slough[1], Bruno Carmo[1], Tristan Barrett[1,2]

1 Department of Radiology, Addenbrooke's Hospital and University of Cambridge, Cambridge, United Kingdom, **2** CamPARI Prostate Cancer Group, Addenbrooke's Hospital and University of Cambridge, Cambridge, United Kingdom

☯ These authors contributed equally to this work.
* ns784@medschl.cam.ac.uk

Citation: Sushentsev N, Kaggie JD, Slough RA, Carmo B, Barrett T (2021) Reproducibility of magnetic resonance fingerprinting-based T_1 mapping of the healthy prostate at 1.5 and 3.0 T: A proof-of-concept study. PLoS ONE 16(1): e0245970. https://doi.org/10.1371/journal.pone.0245970

Editor: Pierpaolo Alongi, Fondazione Istituto G. Giglio di Cefalu, ITALY

Received: August 28, 2020

Accepted: January 11, 2021

Published: January 29, 2021

Data Availability Statement: The data underlying this study are available on Mendeley (DOI: 10.17632/pgfrksc9z5.1).

Funding: The authors acknowledge support from National Institute of Health Research Cambridge Biomedical Research Centre, Cancer Research UK (Cambridge Imaging Centre grant number C197/A16465), the Engineering and Physical Sciences Research Council Imaging Centre in Cambridge and Manchester, and the Cambridge Experimental

Abstract

Facilitating clinical translation of quantitative imaging techniques has been suggested as means of improving interobserver agreement and diagnostic accuracy of multiparametric magnetic resonance imaging (mpMRI) of the prostate. One such technique, magnetic resonance fingerprinting (MRF), has significant competitive advantages over conventional mapping techniques in terms of its multi-site reproducibility, short scanning time and inherent robustness to motion. It has also been shown to improve the detection of clinically significant prostate cancer when added to standard mpMRI sequences, however, the existing studies have all been conducted on 3.0 T MRI systems, limiting the technique's use on 1.5 T MRI scanners that are still more widely used for prostate imaging across the globe. The aim of this proof-of-concept study was, therefore, to evaluate the cross-system reproducibility of prostate MRF T_1 in healthy volunteers (HVs) using 1.5 and 3.0 T MRI systems. The initial validation of MRF T_1 against gold standard inversion recovery fast spin echo (IR-FSE) T_1 in the ISMRM/NIST MRI system revealed a strong linear correlation between phantom-derived MRF and IR-FSE T_1 values was observed at both field strengths ($R^2 = 0.998$ at 1.5T and $R^2 = 0.993$ at 3T; $p = < 0.0001$ for both). In young HVs, inter-scanner CVs demonstrated marginal differences across all tissues with the highest difference of 3% observed in fat (2% at 1.5T vs 5% at 3T). At both field strengths, MRF T_1 could confidently differentiate prostate peripheral zone from transition zone, which highlights the high quantitative potential of the technique given the known difficulty of tissue differentiation in this age group. The high cross-system reproducibility of MRF T_1 relaxometry of the healthy prostate observed in this preliminary study, therefore, supports the technique's prospective clinical validation as part of larger trials employing 1.5 T MRI systems, which are still widely used clinically for routine mpMRI of the prostate.

Cancer Medicine Centre. The funders had no role in study design, data collection and analysis, decision to publish, or preparation of the manuscript.

Competing interests: The authors have declared that no competing interests exist.

Introduction

Multiparametric magnetic resonance imaging (mpMRI) has recently been adopted by major European and American prostate cancer (PCa) guidelines as the key diagnostic tool for detection, local staging and active surveillance of the disease [1, 2]. Despite significant advantages over the traditional systematic biopsy pathway, such as high negative predictive value for clinically significant PCa, mpMRI has limitations including a known learning curve and considerable interobserver variation for image assessment, even amongst experience readers [3–8]. Making prostate MRI more objective by facilitating clinical translation of quantitative imaging techniques is viewed by many experts as key to solving the aforementioned challenges [9, 10]. This move is also supported by the Prostate Imaging Reporting and Data System (PI-RADS) steering committee with a view to complement the current recommendations that are based exclusively on qualitative visual assessment of images [11, 12].

MR fingerprinting is a rapidly developing quantitative imaging technique enabling fast and simultaneous generation of tissue T_1 and T_2 property maps that are inherently spatially registered and robust to motion [13, 14]. The key competitive advantages of MRF over standard mapping techniques, which also make it attractive for PCa imaging, include its higher multisite reproducibility and significantly shorter acquisition time, which is important given the current move towards developing abbreviated prostate imaging protocols in order to reduce scanning times whilst maintaining quality [14–19].

Several pilot studies investigating the added value of MRF to prostate mpMRI have demonstrated significantly improved detection of clinically significant peripheral zone (PZ) and transition zone (TZ) tumors when MRF was used in combination with apparent diffusion coefficient (ADC) mapping [20–23]. However, wider clinical validation of MRF as part of an mpMRI protocol is limited by the fact studies have only validated performance on 3T MRI systems, whist the majority of prostate mpMRI scans even in developed countries are still performed on 1.5T scanners [24–27]. The most recent version of the PI-RADS guidelines (v2.1) suggest that both 1.5T and 3T allow for reliable diagnostic exams in the context of adequate hardware and software, and when optimal acquisition parameters are ensured. [10]

Whilst MRF at both 1.5T and 3T has been used in cardiac and brain imaging, there are surprisingly few studies dedicated to cross-system validation of MRF in different body areas other than the brain [28–30]. It is known that longitudinal T_1 relaxation times are more sensitive to an increase of the magnetic field strength compared to T_2 relaxation and quantitative magnetisation transfer parameters [31]. In the prostate, which generally has longer T_1 values compared to other pelvic and abdominal organs, field-dependent variation of T_1 can reach up to 24%, which may affect the cross-system reproducibility of MRF [15, 32].

Therefore, the objective of this proof-of-concept study was to evaluate the cross-system reproducibility of MRF-based T_1 mapping of the healthy prostate with data acquired from both phantoms and healthy volunteers using 1.5T and 3T MRI systems.

Methods

Phantom study

To evaluate the accuracy of the introduced T_1 and T_2 measurements, MRF and standard relaxation mapping data were obtained from the ISMRM/NIST phantom. [27] Phantom data were obtained on 1.5T MR450 and 3T MR750w scanners (both GE Healthcare, Waukesha, WI, USA) using a 32-channel receiver coil. Regions-of-interest (ROIs) were created from the spheres in either the T_1 or T_2 layer of the phantom. MR Fingerprinting was performed as further described in section 2.4.

Conventional T_1 and T_2 mapping was performed with inversion recovery fast spin echo (IR-FSE) and multiple spin echo (MSE) imaging, respectively. The field-of-view (FOV) = 260x260 mm^2, matrix = 256x256 and slice thickness = 3 mm matched in all techniques. For 2D IR-FSE T_1 mapping, data were acquired with inversion times (TIs) of 50, 100, 200, 400, 800, 1600, and 2400 ms. The IR-FSE sequence used a repetition time (TR) = 8000 ms and echo time (TE) = 13 ms at both 1.5 T and 3.0 T. T_1 data for all non-MRF techniques were fit using non-linear fitting of the signal equations in Python. Multiple spin echo (MSE) data for T_2 estimations were acquired with TEs = 8.1, 16.3, 24.4, 32.6, 40.7, 58.9, 57.0, 65.2 ms. MSE data were fit with a log linear least squares algorithm. The acquisition matched the FOV, matrix, and slices as the MRF acquisition.

Healthy volunteers study

All elements of this prospective study were carried out in accordance with the Declaration of Helsinki and were approved by the institutional ethics board (NRES Committee East of England, UK), with written informed consent obtained from all participants. The volunteers were aged at least 18 years were included in this study, with the exclusion criteria being previous diagnosis or treatment for prostate cancer and clinical contraindication to MRI.

Anatomical imaging

Healthy volunteers underwent prostate MRI on the same 1.5T MR450 and 3T MR750 scanners (both GE Healthcare, Waukesha, WI, USA) used in the phantom study. As per clinical mpMRI acquisition, the protocol included Axial T1 and multiplanar high-resolution T2-weighted 2D fast recovery FSE (FOV = 18x18 cm; voxel size 0.35x0.35 mm2; slice thickness = 3–4 mm; gap = 0–0.5 mm). Diffusion-weighted imaging (DWI) was performed using a spin-echo echo-planar imaging pulse sequence (FOV 28cm; slice thickness 3mm; gap 0mm; b-values: b-150, b-750, and b-1,400 s/mm^2) and an additional small FOV (24 cm) b-2,000s/mm^2 DWI sequence; apparent diffusion coefficient (ADC) maps were calculated automatically.

MR fingerprinting protocol

MRF at both 1.5 T and 3.0 T was acquired with an inversion-prepared 2D steady-state-free-precession (SSFP) MRF sequence [13]. The acquisition consisted of 979 undersampled interleaved spirals with 656 points per spiral, and with sequential spirals rotated by the golden angle. The maximum gradient strength per spiral was 28 mT/m and the maximum slew rate was 108 T/m/s. The imaging parameters were: field-of-view (FOV) = 260x260 mm^2, matrix = 256x256, slices = 3 for ISMRM/NIST imaging and 12–14 for *in vivo* imaging, *in vivo* slice thickness = 6 mm and 3 mm at 1.5T and 3T, respectively, spacing = 5mm and 6mm at 1.5T and 3T (39 mm for both for ISMRM/NIST imaging), respectively, sampling bandwidth = ±250 kHz, slice dephasing = 8π, echo time (TE) = 2.5 ms, repetition time (TR) = 10 ms, acquisition time = 9.79 seconds/slice. The flip angle lists matched those in Jiang et al. [33]. Axial images were acquired to match the standard acquisition planes for other prostate image assessments.

Image analysis

MRF T_1 values for the whole prostate, peripheral zone (PZ), transition zone (TZ), internal obturator muscle and adipose tissue in the ischioanal fossa were calculated from ROIs drawn by a single fellowship-trained uro-radiologist using the open-source segmentation software

ITK-SNAP [34]. ROIs were drawn using anatomical T2WI as reference and subsequently transposed on to the MRF T_1 with their size and location being matched to the appropriate FOV parameters and anatomical position of the outlined structures using in-house software developed within Python using the PyQtGraph and PyDicom libraries [35].

Statistics

In the phantom study, simple linear regression was used to evaluate the relationship between T_1 and T_2 values obtained using IR-FSE, MSE and MRF mapping techniques with their agreement assessed using Bland-Altman analysis. In the healthy volunteers study, the D'Agostino and Pearson test was applied to assess the distribution of imaging values with their intergroup comparison performed using either paired t-test or Wilcoxon matched-pairs signed rank test as appropriate. Both in the phantom and healthy volunteers studies, the variation of imaging values as a means of their cross-system reproducibility was evaluated using a coefficient of variation (CV). All plots and figures were created in Prism 8 (GraphPad Software, San Diego, CA).

Results

Phantom study

Summary mean inter-scanner T_1 and T_2 values obtained from the corresponding ISMRM/NIST phantom layers using MRF, inversion recovery fast spin echo (IR-FSE) and multiple spin echo (MSE) imaging are presented in **Table 1**. Paired t-test showed no inter-scanner differences between IR-FSE and MRF-based T_1 phantom values ($p = 0.795$ and $p = 0.102$, respectively). As a measure of reproducibility, coefficients of variations (CVs) were calculated and are also presented in **Table 1**, showing inter-scanner differences of 0.17% and 2.57% for IR-FSE and MRF T_1, respectively. Inter-scanner T_2 values obtained using MRF and MSE imaging were, however, significantly different in both cases ($p = 0.0002$ and $p = 0.0006$, respectively) with differences in their CVs reaching 0.10% and 7.66%, respectively.

Fig 1A and **1B** show the mean ISMRM/NIST phantom MRF T_1 values plotted against T_1 values obtained using inversion recovery fast spin echo (IR-FSE) imaging at 1.5T and 3T, respectively. The analysis showed a strong linear correlation between MRF and IR-FSE at both field strengths ($R^2 = 0.998$ at 1.5T and $R^2 = 0.993$ at 3T; $p = < 0.0001$ for both) with slopes of the linear fits and y-intercepts presented in the corresponding figures. The Bland-Altman analysis revealed good agreement between the two techniques at both 1.5T and 3T with the corresponding mean bias and 95% limits of agreement (LOA) presented in **Fig 1D** and **1E**, respectively. When plotted against each other, MRF T_1 values obtained at 1.5T and 3T also demonstrated a strong linear correlation ($R^2 = 0.994$; $p < 0.0001$) and acceptable agreement

Table 1. Summary ISMRM/NIST phantom T_1 and T_2 relaxation times and coefficients of variation obtained using inversion recovery fast spin echo (IR-FSE), multiple spin echo (MSE) and magnetic resonance fingerprinting (MRF) at 1.5T and 3T systems.

	Mean ± SD			Coefficient of variation (%)	
Sequence	**1.5T**	**3T**	***P***	**1.5T**	**3T**
IR-FSE T_1	616.1 ± 400.9	615.8 ± 401.8	0.7951	65.08	65.25
MRF T_1	559.3 ± 402.2	544.1 ± 405.3	0.1019	71.91	74.48
MSE T_2	137.8 ± 112.2	92.8 ± 82.7	0.0002	116.80	116.90
MRF T_2	471.2 ± 550.2	95.6 ± 111.8	0.0006	81.46	89.12

SD = standard deviation.

https://doi.org/10.1371/journal.pone.0245970.t001

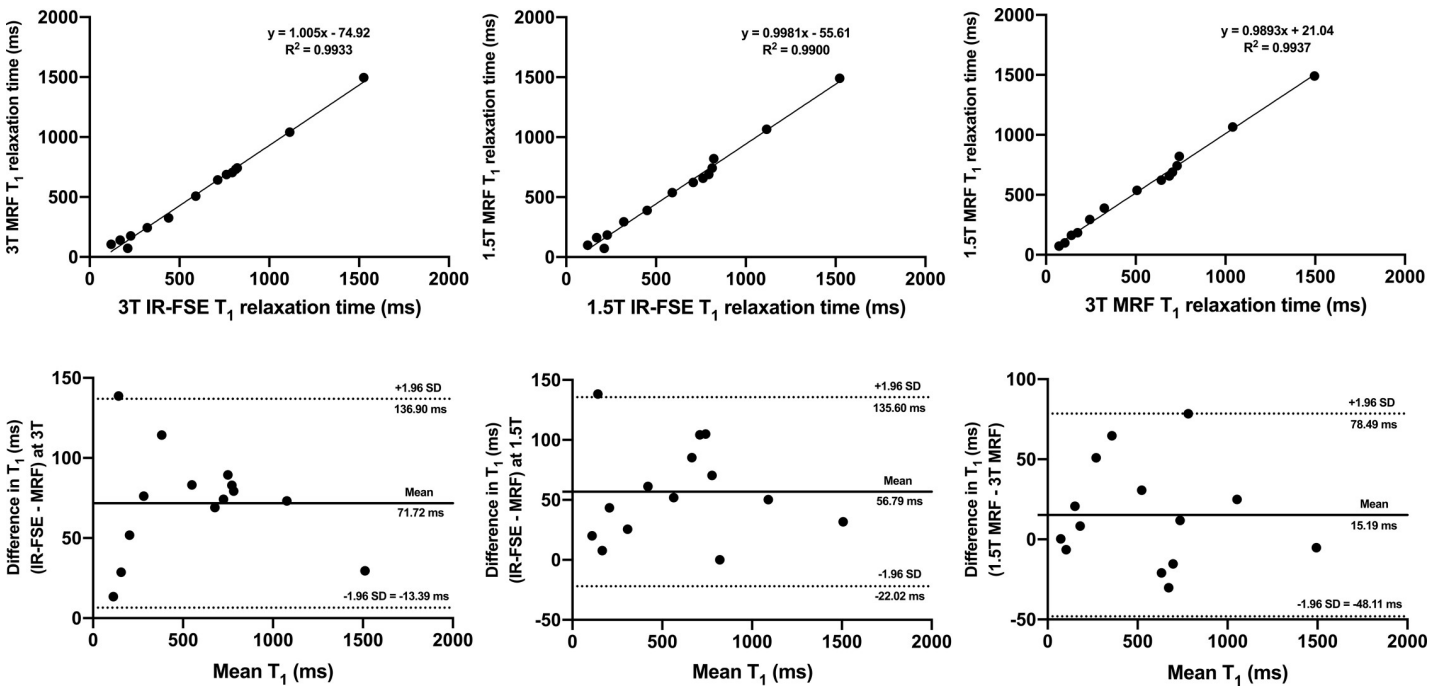

Fig 1. Linear regression plots (a-c) and Bland-Altman plots (d-f) comparing MRF T_1 ISMRM/NIST phantom values with those obtained using IR-FSE at 3T (a, d) and 1.5T (b, e). An inter-scanner comparison of MRF T_1 values is also presented (c, f). On Fig (d-f), dotted lines represent upper and lower 95% limits of agreement and bold lines represent the mean biases with appropriate captions included. MRF = magnetic resonance fingerprinting, IR-FSE = inversion recovery fast spin echo, SD = standard deviation.

https://doi.org/10.1371/journal.pone.0245970.g001

(bias 15.19 ms, 95% LOA -48.11 ms to 78.49 ms) with corresponding plots presented in Fig 1C and 1F, respectively.

The outcomes of a similar analysis comparing the MRF and multiple spin echo (MSE) T_2 values obtained at 1.5T and 3T are presented in Fig 2. It is of note that T_2 values obtained in this study showed consistently poorer reproducibility as demonstrated by both linear regression and Bland-Altman analysis, prompting us to focus the following presentation and analysis of the *in vivo* results on T_1 relaxometry.

Healthy volunteers study

The study included 10 healthy male volunteers (mean age 32.3 years, range 24–41) who underwent MRF of the prostate at 1.5T and 3T within the same imaging session.

Summary mean inter-scanner MRF T_1 values and coefficients of variation (CVs) obtained from the whole prostate, peripheral zone (PZ), transition zone (TZ), internal obturator muscle and fat in the ischioanal fossa are presented in Table 2. As expected, 3T MRF T_1 values were significantly longer in all tissues compared to 1.5T MRF ($P < 0.0001$ for all). Inter-scanner CVs demonstrated only marginal differences in all tissues with the highest difference of 3% observed in fat (2% at 1.5T vs 5% at 3T). T_1 values obtained from the PZ showed the highest overall variation with CVs at 1.5T and 3T being 10.9% and 10.3%, respectively. The outcomes of a similar analysis conducted for *in vivo* MRF T_2 relaxometry is presented in S1 Table.

Albeit weaker than in the phantom experiment, a strong linear correlation was noted between the combined *in vivo* 1.5T and 3T MRF T_1 values obtained from all tissues included in the analysis ($R^2 = 0.914$; $p < 0.0001$); Fig 3A. Fig 3B illustrates the inter-scanner agreement between MRF T_1 relaxation times (bias 602.1 ms, 95% LOA 72.0 ms to 1132.0 ms) with only a

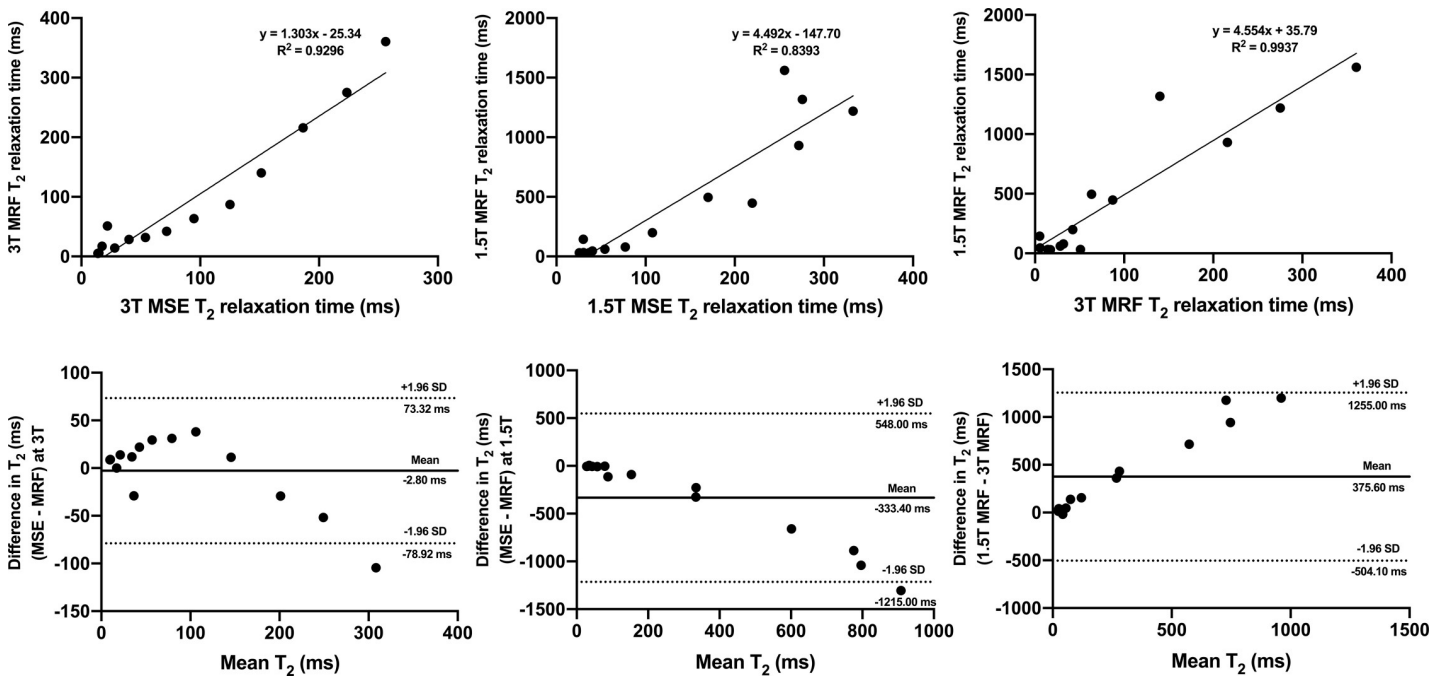

Fig 2. Linear regression plots (a-c) and Bland-Altman plots (d-f) comparing MRF T_2 ISMRM/NIST phantom values with those obtained using MSE at 3T (a, d) and 1.5T (b, e). An inter-scanner comparison of MRF T_2 values is also presented (c, f). On Fig (d-f), dotted lines represent upper and lower 95% limits of agreement and bold lines represent the mean biases with appropriate captions included. MRF = magnetic resonance fingerprinting, MSE = multiple spin echo, SD = standard deviation.

https://doi.org/10.1371/journal.pone.0245970.g002

single value being outside the 95% LOA. The outcomes of the Bland-Altman analysis for each individual tissue are presented in Fig 4, with acceptable agreement noted for all tissues included in the analysis. S2 and S3 **Figs** depict the outcomes of a similar analysis for MRF T_2 relaxometry.

At both 1.5T and 3T, MRF T_1 relaxometry enabled confident differentiation between the whole prostate, PZ and TZ (Fig 5). It is of note that the difference between MRF T_1 relaxation times derived from PZ and TZ was slightly more prominent at 3T (24%) compared to 1.5T (19%). S3 Fig demonstrates the outcomes of a similar comparison for MRF T_2 relaxometry.

Discussion

This prospective proof-of-concept study investigated the cross-system reproducibility of SSFP MRF T_1 of the prostate in healthy volunteers who were scanned using 1.5T and 3T systems

Table 2. Summary MRF T_1 relaxation times and coefficients of variation obtained at 1.5T and 3T from the whole prostate, peripheral zone, transition zone, internal obturator muscle and fat from the ischioanal fossa.

	Mean ± SD			Coefficient of variation (%)	
Tissue	**1.5T**	**3T**	***P***	**1.5T**	**3T**
Prostate	1054.0 ± 80.1	1769.0 ± 112.7	< 0.0001	7.60	6.37
Peripheral zone	1202.0 ± 131.3	2041.0 ± 209.4	< 0.0001	10.93	10.26
Transition zone	968.8 ± 60.7	1552.0 ± 105.2	< 0.0001	6.26	6.78
Muscle	725.6 ± 23.8	1446.0 ± 73.95	< 0.0001	3.29	5.12
Fat	192.1 ± 3.8	345.1 ± 17.1	< 0.0001	1.99	4.96

SD = standard deviation.

https://doi.org/10.1371/journal.pone.0245970.t002

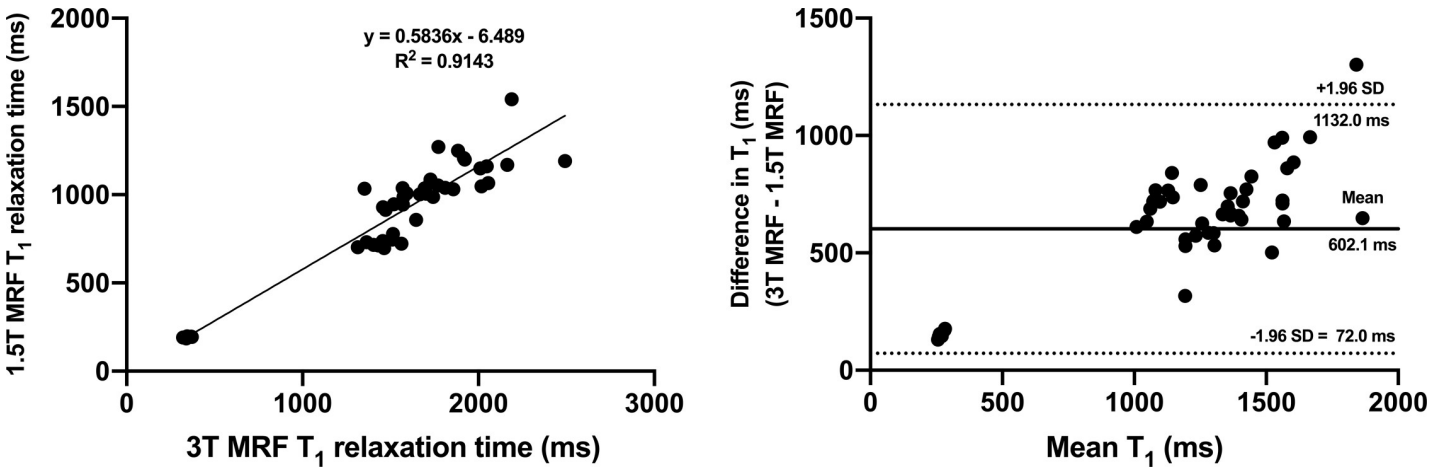

Fig 3. Linear regression (a) and Bland-Altman (b) plots comparing in vivo MRF T_1 values obtained from all tissues combined at 1.5T and 3T systems. On Fig (b), dotted lines represent upper and lower 95% limits of agreement and bold lines represent the mean biases with appropriate captions included. MRF = magnetic resonance fingerprinting, SD = standard deviation.

https://doi.org/10.1371/journal.pone.0245970.g003

with the same sequence parameters and reconstruction methods. The study was preceded by a phantom experiment that confirmed high reliability of MRF T_1 mapping used when validated against IR-FSE imaging. The healthy volunteers study revealed acceptable inter-scanner agreement and excellent reproducibility of MRF T_1 relaxometry in all tissues. At 3T, the magnitude of difference between MRF T_1 obtained from the peripheral and transition zones of the prostate was slightly higher than at 1.5T, being, however, within the limits of statistical significance at both field strengths. These results, therefore, support further validation of prostate MRF at 1.5T as part of a standard-of-care mpMRI protocol.

To our knowledge, this is the first study to report MRF of the prostate performed at 1.5T, which is still commonly used for routine prostate imaging [26]. The observed high cross-system reproducibility of prostate MRF T_1 is similar to that reported in the brain by Buonincontri *et al*., suggesting the overall robustness of MRF to field-dependent variation of T_1 [30]. Our 3T MRF T_1 values obtained from the healthy PZ and TZ are similar to those obtained in a patient population by other authors (2247.0 ms ± 450 ms for PZ [22] and 1800 ms ± 150 ms for TZ [20]) with subtle differences being expected due to the known age-related changes in histological and imaging features of the prostate [36, 37]. The observed ability of MRF to differentiate PZ and TZ in healthy volunteers at both 1.5T and 3T highlights MRF's sensitivity to the underlying tissue organisation, which may be even more prominent in the older patients, in whom even visual differentiation of the prostatic zones is much less challenging [36, 38].

These preliminary results pave the way for future studies investigating the diagnostic performance of prostate MRF at 1.5T. It is known that prostate mpMRI at 1.5T is able to produce T_2-weighted images of comparable diagnostic quality, however, the key argument in favour of 3T imaging is its ability to achieve higher signal-to-noise and contrast-to-noise ratios for diffusion-weighted imaging (DWI), which is the key sequence for PZ assessment, enabling DWI at higher b-values [39–42]. If 1.5T MRF retains its added value to ADC mapping previously demonstrated at 3T, it can potentially compensate for the inherent inferiority of DWI at 1.5T [20–22]. Furthermore, MRF's inherent robustness to motion may help further establish its role as an auxiliary sequence to DWI, which is often degraded by motion artefact or rectal loading [43–46]. Finally, the added value of quantitative MRI can be harnessed clinically in the active surveillance setting where time-series change of tumour-derived relaxometry can serve as a more objective means of tracking the disease progression [47].

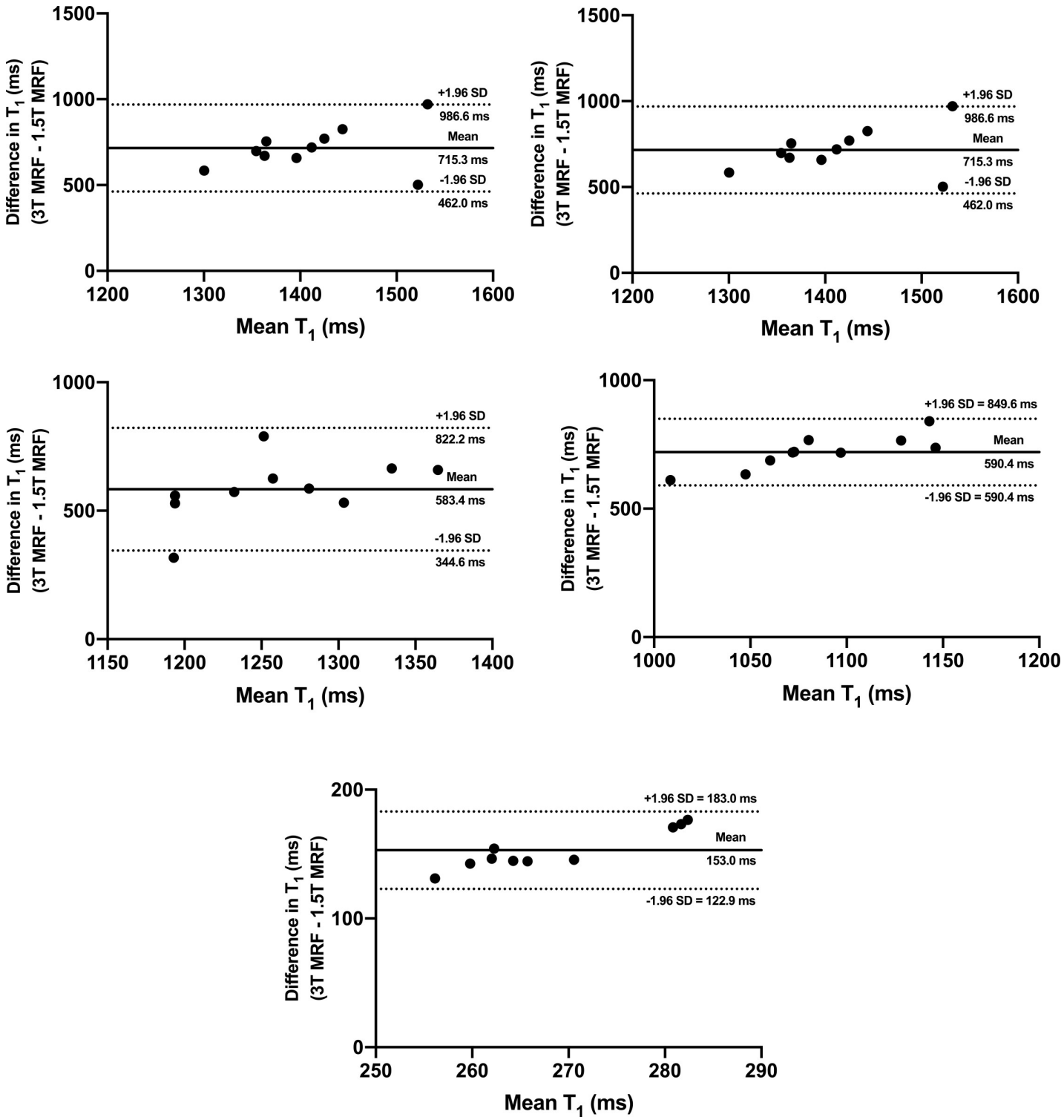

Fig 4. Bland-Altman plots comparing in vivo MRF T_1 values obtained from the whole prostate (a), peripheral zone (b), transition zone (c), internal obturator muscle (d) and fat in the ischioanal fossa (e) at 1.5T and 3T systems. Dotted lines represent upper and lower 95% limits of agreement and bold lines represent the mean biases with appropriate captions included. MRF = magnetic resonance fingerprinting, SD = standard deviation.

https://doi.org/10.1371/journal.pone.0245970.g004

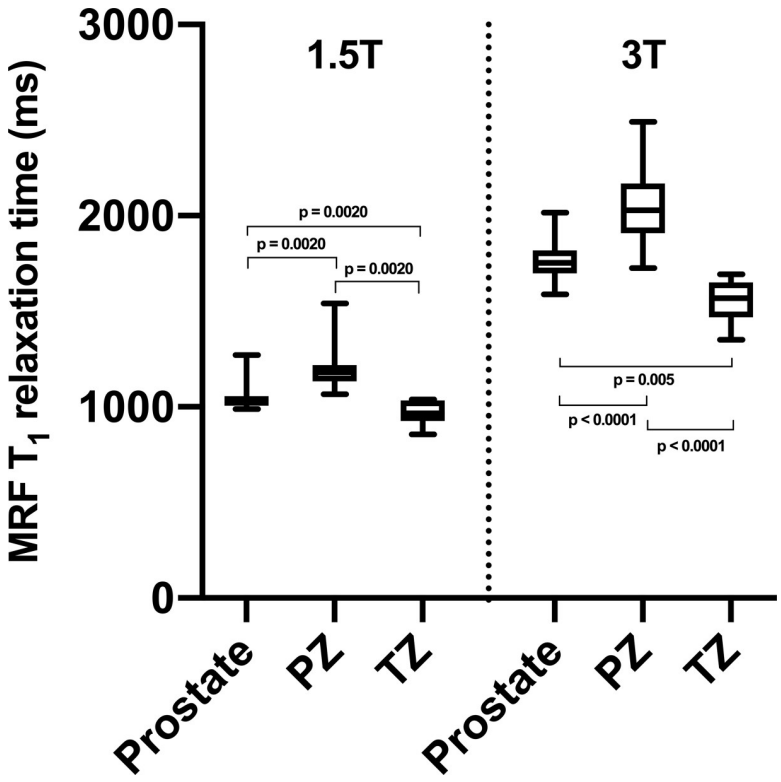

Fig 5. Box-and-whiskers plots representing MRF T_1 relaxation times obtained from the whole prostate, peripheral zone (PZ) and transition zone (TZ) at 1.5T and 3T (left and right sides of the graph, respectively). Top and bottom of boxes represent 25th and 75th percentiles of data, respectively; line in boxes represents the median value and bars represent minimum and maximum values. MRF = magnetic resonance fingerprinting.

https://doi.org/10.1371/journal.pone.0245970.g005

Our study has some limitations. The healthy volunteers study population was a small cohort of healthy volunteers of a younger age than typical patients with PCa. Although this may have introduced age-related heterogeneity, the reported high cross-system reproducibility of MRF is further complemented by its ability to differentiate normal PZ and TZ, which is considered less straightforward in younger adults [48]. Furthermore, the inclusion of older adults would limit our ability to sample healthy prostatic tissue due to high prevalence of benign conditions such as benign prostatic hyperplasia and prostatitis, or even undiagnosed PCa in otherwise healthy older men [49, 50]. To achieve comparable image quality, MRF at 1.5T was acquired with higher slice thickness and gap than at 3T, however, this mirrors standard clinical practice [51]. Having shown broadly similar results, MRF T_2 mapping was unreliable in this study, and stronger consideration will be given in future studies to methods increasing its signal-to-noise ratio and improving the pattern matching algorithms.

In conclusion, the excellent reproducibility and high cross-system agreement of MRF T_1 relaxometry of the healthy prostate observed in this preliminary study support the technique's prospective clinical validation on 1.5T MRI systems. The reported findings could be used to justify further investigations for incorporating MRF into clinical prostate MRI protocols, larger population studies, and multi-site/multi-vendor investigations. If this method can be translated into clinical practice and improve both the speed and diagnostic value of imaging, it would add significant value given the current unprecedented demand on imaging services.

Supporting information

S1 Table. Summary MRF T_2 relaxation times and coefficients of variation obtained at 1.5T and 3T from the whole prostate, peripheral zone, transition zone, internal obturator muscle and fat from the ischioanal fossa. SD = standard deviation.
(DOCX)

S1 Fig. Linear regression (a) and Bland-Altman (b) plots comparing in vivo MRF T2 values obtained from all tissues combined at 1.5T and 3T systems. On Fig (b), dotted lines represent upper and lower 95% limits of agreement and bold lines represent the mean biases with appropriate captions included. MRF = magnetic resonance fingerprinting, SD = standard deviation.
(TIF)

S2 Fig. Bland-Altman plots comparing in vivo MRF T2 values obtained from the whole prostate (a), peripheral zone (b), transition zone (c), internal obturator muscle (d) and fat in the ischioanal fossa (e) at 1.5T and 3T systems. Dotted lines represent upper and lower 95% limits of agreement and bold lines represent the mean biases with appropriate captions included. MRF = magnetic resonance fingerprinting, SD = standard deviation.
(TIF)

S3 Fig. Box-and-whiskers plots representing MRF T2 relaxation times obtained from the whole prostate, peripheral zone (PZ) and transition zone (TZ) at 1.5T and 3T (left and right sides of the graph, respectively). Top and bottom of boxes represent 25th and 75th percentiles of data, respectively; line in boxes represents the median value and bars represent minimum and maximum values. MRF = magnetic resonance fingerprinting.
(TIF)

Author Contributions

Conceptualization: Nikita Sushentsev, Joshua D. Kaggie, Tristan Barrett.

Data curation: Nikita Sushentsev, Joshua D. Kaggie.

Formal analysis: Nikita Sushentsev.

Investigation: Joshua D. Kaggie, Rhys A. Slough, Bruno Carmo, Tristan Barrett.

Methodology: Joshua D. Kaggie.

Project administration: Bruno Carmo, Tristan Barrett.

Resources: Bruno Carmo.

Supervision: Rhys A. Slough, Tristan Barrett.

Writing – original draft: Nikita Sushentsev.

Writing – review & editing: Joshua D. Kaggie, Rhys A. Slough, Bruno Carmo, Tristan Barrett.

References

1. EAU Guidelines: Prostate Cancer | Uroweb. [cited 2 Jun 2020]. Available: https://uroweb.org/guideline/prostate-cancer/
2. Standard Operating Procedure for Multiparametric Magnetic Resonance Imaging in the Diagnosis, Staging and Management of Prostate Cancer—American Urological Association. [cited 2 Jun 2020]. Available: https://www.auanet.org/guidelines/mri-of-the-prostate-sop
3. Gaziev G, Wadhwa K, Barrett T, Koo BC, Gallagher FA, Serrao E, et al. Defining the learning curve for multiparametric magnetic resonance imaging (MRI) of the prostate using MRI-transrectal

ultrasonography (TRUS) fusion-guided transperineal prostate biopsies as a validation tool. BJU Int. 2016; 117: 80–86. https://doi.org/10.1111/bju.12892 PMID: 25099182

4. Le JD, Tan N, Shkolyar E, Lu DY, Kwan L, Marks LS, et al. Multifocality and prostate cancer detection by multiparametric magnetic resonance imaging: Correlation with whole-mount histopathology. Eur Urol. 2015; 67: 569–576. https://doi.org/10.1016/j.eururo.2014.08.079 PMID: 25257029
5. Greer MD, Shih JH, Lay N, Barrett T, Bittencourt L, Borofsky S, et al. Interreader variability of prostate imaging reporting and data system version 2 in detecting and assessing prostate cancer lesions at prostate MRI. Am J Roentgenol. 2019; 212: 1197–1205. https://doi.org/10.2214/AJR.18.20536 PMID: 30917023
6. Rosenkrantz AB, Ginocchio LA, Cornfeld D, Froemming AT, Gupta RT, Turkbey B, et al. Interobserver reproducibility of the PI-RADS version 2 lexicon: A multicenter study of six experienced prostate radiologists. Radiology. 2016; 280: 793–804. https://doi.org/10.1148/radiol.2016152542 PMID: 27035179
7. de Rooij M, Israël B, Tummers M, Ahmed HU, Barrett T, Giganti F, et al. ESUR/ESUI consensus statements on multi-parametric MRI for the detection of clinically significant prostate cancer: quality requirements for image acquisition, interpretation and radiologists' training. Eur Radiol. 2020 [cited 25 Jun 2020]. https://doi.org/10.1007/s00330-020-06929-z PMID: 32424596
8. Barrett T, Padhani AR, Patel A, Ahmed HU, Allen C, Bardgett H, et al. Certification in reporting multiparametric magnetic resonance imaging of the prostate: recommendations of a UK consensus meeting. BJU Int. 2020 [cited 6 Jan 2021]. https://doi.org/10.1111/bju.15285 PMID: 33113258
9. Schieda N, Lim CS, Zabihollahy F, Abreu-Gomez J, Krishna S, Woo S, et al. Quantitative Prostate MRI. J Magn Reson Imaging. 2020; jmri.27191. https://doi.org/10.1002/jmri.27191 PMID: 32410356
10. Panda A, Gulani V. Quantitative Imaging of Prostate: Scope and Future Directions. Reading MRI of the Prostate. Springer International Publishing; 2020. pp. 97–108. https://doi.org/10.1007/978-3-319-99357-7_10
11. Barrett T, Rajesh A, Rosenkrantz AB, Choyke PL, Turkbey B. PI-RADS version 2.1: one small step for prostate MRI. Clinical Radiology. W.B. Saunders Ltd; 2019. pp. 841–852. https://doi.org/10.1016/j.crad.2019.05.019 PMID: 31239107
12. Turkbey B, Rosenkrantz AB, Haider MA, Padhani AR, Villeirs G, Macura KJ, et al. Prostate Imaging Reporting and Data System Version 2.1: 2019 Update of Prostate Imaging Reporting and Data System Version 2. European Urology. Elsevier B.V.; 2019. pp. 340–351. https://doi.org/10.1016/j.eururo.2019.02.033 PMID: 30898406
13. Ma D, Gulani V, Seiberlich N, Liu K, Sunshine JL, Duerk JL, et al. Magnetic resonance fingerprinting. Nature. 2013; 495: 187–192. https://doi.org/10.1038/nature11971 PMID: 23486058
14. McGivney DF, Boyacıoğlu R, Jiang Y, Poorman ME, Seiberlich N, Gulani V, et al. Magnetic resonance fingerprinting review part 2: Technique and directions. J Magn Reson Imaging. 2020; 51: 993–1007. https://doi.org/10.1002/jmri.26877 PMID: 31347226
15. Bipin Mehta B, Coppo S, Frances McGivney D, Ian Hamilton J, Chen Y, Jiang Y, et al. Magnetic resonance fingerprinting: a technical review. Magn Reson Med. 2019; 81: 25–46. https://doi.org/10.1002/mrm.27403 PMID: 30277265
16. Poorman ME, Martin MN, Ma D, McGivney DF, Gulani V, Griswold MA, et al. Magnetic resonance fingerprinting Part 1: Potential uses, current challenges, and recommendations. Journal of Magnetic Resonance Imaging. John Wiley and Sons Inc.; 2020. pp. 675–692. https://doi.org/10.1002/jmri.26836 PMID: 31264748
17. Sushentsev N, Caglic I, Sala E, Shaida N, Slough RA, Carmo B, et al. The effect of capped biparametric magnetic resonance imaging slots on weekly prostate cancer imaging workload. Br J Radiol. 2020; 93: 20190929. https://doi.org/10.1259/bjr.20190929 PMID: 31971823
18. van der Leest M, Israël B, Cornel EB, Zámecnik P, Schoots IG, van der Lelij H, et al. High Diagnostic Performance of Short Magnetic Resonance Imaging Protocols for Prostate Cancer Detection in Biopsy-naïve Men: The Next Step in Magnetic Resonance Imaging Accessibility. Eur Urol. 2019; 76: 574–581. https://doi.org/10.1016/j.eururo.2019.05.029 PMID: 31167748
19. Zawaideh JP, Sala E, Shaida N, Koo B, Warren AY, Carmisciano L, et al. Diagnostic accuracy of biparametric versus multiparametric prostate MRI: assessment of contrast benefit in clinical practice. Eur Radiol. 2020;30. https://doi.org/10.1007/s00330-020-06782-0 PMID: 32166495
20. Panda A, Obmann VC, Lo WC, Margevicius S, Jiang Y, Schluchter M, et al. MR fingerprinting and ADC mapping for characterization of lesions in the transition zone of the prostate gland. Radiology. 2019; 292: 685–694. https://doi.org/10.1148/radiol.2019181705 PMID: 31335285
21. Yu AC, Badve C, Ponsky LE, Pahwa S, Dastmalchian S, Rogers M, et al. Development of a Combined MR Fingerprinting and Diffusion Examination for Prostate Cancer. Radiology. 2017; 283: 729–738. https://doi.org/10.1148/radiol.2017161599 PMID: 28187264

22. Panda A, O'connor G, Lo WC, Jiang Y, Margevicius S, Schluchter M, et al. Targeted Biopsy Validation of Peripheral Zone Prostate Cancer Characterization With Magnetic Resonance Fingerprinting and Diffusion Mapping. Invest Radiol. 2019; 54: 485–493. https://doi.org/10.1097/RLI.0000000000000569 PMID: 30985480

23. Sushentsev N, Kaggie JD, Buonincontri G, Schulte RF, Graves MJ, Gnanapragasam VJ, et al. The effect of gadolinium-based contrast agent administration on magnetic resonance fingerprinting-based T1 relaxometry in patients with prostate cancer. Sci Rep. 2020;10. https://doi.org/10.1038/s41598-019-56089-4 PMID: 32001736

24. Hegde J V., Mulkern R V., Panych LP, Fennessy FM, Fedorov A, Maier SE, et al. Multiparametric MRI of prostate cancer: An update on state-of-the-art techniques and their performance in detecting and localizing prostate cancer. Journal of Magnetic Resonance Imaging. NIH Public Access; 2013. pp. 1035–1054. https://doi.org/10.1002/jmri.23860 PMID: 23606141

25. Magnetic resonance imaging (MRI) equipment, operations and planning in the NHS Report from the Clinical Imaging Board. 2017. Available: www.ipem.ac.ukwww.sor.org

26. Davies C, Castle JT, Stalbow K, Haslam PJ. Prostate mpMRI in the UK: the state of the nation. Clin Radiol. 2019; 74: 894.e11–894.e18. https://doi.org/10.1016/j.crad.2019.09.129 PMID: 31627803

27. Brizmohun Appayya M, Adshead J, Ahmed HU, Allen C, Bainbridge A, Barrett T, et al. National implementation of multi-parametric magnetic resonance imaging for prostate cancer detection–recommendations from a UK consensus meeting. BJU International. Blackwell Publishing Ltd; 2018. pp. 13–25. https://doi.org/10.1111/bju.14361 PMID: 29699001

28. Hamilton JI, Jiang Y, Chen Y, Ma D, Lo WC, Griswold M, et al. MR fingerprinting for rapid quantification of myocardial T1, T2, and proton spin density. Magn Reson Med. 2017; 77: 1446–1458. https://doi.org/10.1002/mrm.26216 PMID: 27038043

29. Cruz G, Jaubert O, Botnar RM, Prieto C. Cardiac Magnetic Resonance Fingerprinting: Technical Developments and Initial Clinical Validation. Current Cardiology Reports. Current Medicine Group LLC 1; 2019. pp. 1–10. https://doi.org/10.1007/s11886-019-1086-z PMID: 30631962

30. Buonincontri G, Biagi L, Retico A, Cecchi P, Cosottini M, Gallagher FA, et al. Multi-site repeatability and reproducibility of MR fingerprinting of the healthy brain at 1.5 and 3.0 T. Neuroimage. 2019; 195: 362–372. https://doi.org/10.1016/j.neuroimage.2019.03.047 PMID: 30923028

31. Stanisz GJ, Odrobina EE, Pun J, Escaravage M, Graham SJ, Bronskill MJ, et al. T 1, T 2 Relaxation and Magnetization Transfer in Tissue at 3T. 2005 [cited 2 Jun 2020]. https://doi.org/10.1002/mrm.20605 PMID: 16086319

32. De Bazelaire CMJ, Duhamel GD, Rofsky NM, Alsop DC. MR Imaging Relaxation Times of Abdominal and Pelvic Tissues Measured in Vivo at 3.0 T: Preliminary Results. Radiology. 2004; 230: 652–659. https://doi.org/10.1148/radiol.2303021331 PMID: 14990831

33. Jiang Y, Ma D, Seiberlich N, Gulani V, Griswold MA. MR fingerprinting using fast imaging with steady state precession (FISP) with spiral readout. Magn Reson Med. 2015; 74: 1621–1631. https://doi.org/10.1002/mrm.25559 PMID: 25491018

34. Yushkevich PA, Piven J, Hazlett HC, Smith RG, Ho S, Gee JC, et al. User-guided 3D active contour segmentation of anatomical structures: Significantly improved efficiency and reliability. Neuroimage. 2006; 31: 1116–1128. https://doi.org/10.1016/j.neuroimage.2006.01.015 PMID: 16545965

35. Mason D. SU-E-T-33: Pydicom: An Open Source DICOM Library. Med Phys. 2011; 38: 3493–3493. https://doi.org/10.1118/1.3611983

36. De Visschere PJL, Vral A, Perletti G, Pattyn E, Praet M, Magri V, et al. Multiparametric magnetic resonance imaging characteristics of normal, benign and malignant conditions in the prostate. Eur Radiol. 2017; 27: 2095–2109. https://doi.org/10.1007/s00330-016-4479-z PMID: 27491874

37. Zhang J, Tian WZ, Hu CH, Niu TL, Wang XL, Chen XY. Age-related changes of normal prostate: Evaluation by MR diffusion tensor imaging. Int J Clin Exp Med. 2015; 8: 11220–11224. Available: www.ijcem.com/ PMID: 26379927

38. Allen KS, Kressel HY, Arger PH, Pollack HM. Age-related changes of the prostate: Evaluation by MR imaging. Am J Roentgenol. 1989; 152: 77–81. https://doi.org/10.2214/ajr.152.1.77 PMID: 2783293

39. Van Nieuwenhove S, Saussez TP, Thiry S, Trefois P, Annet L, Michoux N, et al. Prospective comparison of a fast 1.5-T biparametric with the 3.0-T multiparametric ESUR magnetic resonance imaging protocol as a triage test for men at risk of prostate cancer. BJU Int. 2019; 123: 411–420. https://doi.org/10.1111/bju.14538 PMID: 30240059

40. Shah ZK, Elias SN, Abaza R, Zynger DL, DeRenne LA, Knopp M V., et al. Performance Comparison of 1.5-T Endorectal Coil MRI with 3.0-T Nonendorectal Coil MRI in Patients with Prostate Cancer. Acad Radiol. 2015; 22: 467–474. https://doi.org/10.1016/j.acra.2014.11.007 PMID: 25579637

41. Ullrich T, Quentin M, Oelers C, Dietzel F, Sawicki LM, Arsov C, et al. Magnetic resonance imaging of the prostate at 1.5 versus 3.0 T: A prospective comparison study of image quality. Eur J Radiol. 2017; 90: 192–197. https://doi.org/10.1016/j.ejrad.2017.02.044 PMID: 28583633

42. Engels RRM, Israël B, Padhani AR, Barentsz JO. Multiparametric Magnetic Resonance Imaging for the Detection of Clinically Significant Prostate Cancer: What Urologists Need to Know. Part 1: Acquisition. Eur Urol. 2020; 77: 457–468. https://doi.org/10.1016/j.eururo.2019.09.021 PMID: 31582290

43. Caglic I, Hansen NL, Slough RA, Patterson AJ, Barrett T. Evaluating the effect of rectal distension on prostate multiparametric MRI image quality. Eur J Radiol. 2017; 90: 174–180. https://doi.org/10.1016/j.ejrad.2017.02.029 PMID: 28583630

44. Slough RA, Caglic I, Hansen NL, Patterson AJ, Barrett T. Effect of hyoscine butylbromide on prostate multiparametric {MRI} anatomical and functional image quality. Clin Radiol. 2018; 73: 216.e9—216.e14. https://doi.org/10.1016/j.crad.2017.07.013 PMID: 28803622

45. Hsieh JJL, Svalbe I. Magnetic resonance fingerprinting: from evolution to clinical applications. J Med Radiat Sci. 2020; jmrs.413. https://doi.org/10.1002/jmrs.413 PMID: 32596957

46. Barrett T, Lawrence EM, Priest AN, Warren AY, Gnanapragasam VJ, Gallagher FA, et al. Repeatability of diffusion-weighted MRI of the prostate using whole lesion ADC values, skew and histogram analysis. Eur J Radiol. 2019; 110: 22–29. https://doi.org/10.1016/j.ejrad.2018.11.014 PMID: 30599864

47. Caglic I, Sushentsev N, Gnanapragasam V, Sala E, Shaida N, Koo B, et al. MRI-derived PRECISE scores for predicting pathologically-confirmed radiological progression in prostate cancer patients on active surveillance. Eur Radiol 2020. 2020; 1–10. https://doi.org/10.1007/s00330-020-07336-0 PMID: 33196886

48. Bura V, Caglic I, Snoj Z, Sushentsev N, Berghe AS, Priest AN, et al. MRI features of the normal prostatic peripheral zone: the relationship between age and signal heterogeneity on T2WI, DWI, and DCE sequences. Eur Radiol. 2021; 1–10. https://doi.org/10.1007/s00330-020-07108-w PMID: 32767103

49. Kitzing YX, Prando A, Varol C, Karczmar GS, Maclean F, Oto A. Benign conditions that mimic prostate carcinoma: MR imaging features with histopathologic correlation. Radiographics. 2016; 36: 162–175. https://doi.org/10.1148/rg.2016150030 PMID: 26587887

50. Bell KJL, Del Mar C, Wright G, Dickinson J, Glasziou P. Prevalence of incidental prostate cancer: A systematic review of autopsy studies. Int J Cancer. 2015; 137: 1749–1757. https://doi.org/10.1002/ijc.29538 PMID: 25821151

51. Burn PR, Freeman SJ, Andreou A, Burns-Cox N, Persad R, Barrett T. A multicentre assessment of prostate MRI quality and compliance with UK and international standards. Clin Radiol. 2019; 74: 894.e19–894.e25. https://doi.org/10.1016/j.crad.2019.03.026 PMID: 31296337